

Asymptotic description of fretting wear and fretting fatigue for incomplete contacts

N. Cwiekala*, D. A. Hills

^a*Department of Engineering Science, University of Oxford, Parks Road, OX1 3PJ Oxford, United Kingdom*

Abstract

Looking at wear of incomplete contacts in partial slip we start from an asymptotic description of the contact tractions at the contact edges. We introduce distributed dislocations along the slip zone to account for the profile reduction due to wear and find the long-term time asymptote where the contact is wholly stuck. The resulting stress field is used to find the crack tip stress intensity factors for short contact edge cracks, which are useful in predicting the crack nucleation threshold.

Keywords: Short cracks, Fretting wear, Fretting fatigue, Asymptotic analyses, Stress intensity factor

Nomenclature

a	contact half-width
B_i	Burgers vector densities
d	Extent of slip zone
f	Coefficient of friction
$g_{I,II}^{1,2}$	functions for remote calibrations
G_{ijk}	Stress Kernel for a dislocation
$K_{I,II}$	Normal and shear stress intensity factor at the wear boundary
$K_{I,II}^c$	Mode I and II crack tip stress intensity factor
K_{II}^e	Asymptotic shear traction stress intensity factor
l	Crack length
L_I	Asymptotic contact pressure multiplier
N	Normal traction along wear-zone or crack faces

*Corresponding author.

Email address: nils.cwiekala@eng.ox.ac.uk (N. Cwiekala)

p	Normal traction along contact interface
p_j	Coefficients for analytical approximation
P	Normal load applied to contact
q	Shear traction along contact interface
q_i	Coefficients for analytical approximation
Q	tangential load applied to contact
r	Distance to contact edge
R	Radius of Hertzian contact cylinder
s_i	Integration points
S	Shear traction along wear-zone or crack faces
t_k	Collocation points
w	Extent of wear-zone
W_i	weights for numerical quadrature
x	Coordinate parallel with crack line
y	Coordinate aligned with contact interface
ϵ	Infinitesimal
θ	Angle measured from contact interface
κ	Kolosov's constant
λ	Eigenvalue for Williams solution
μ	Shear modulus
ν	Poisson's ratio
ξ	Dislocation coordinate in Cartesian coordinate system
ρ	Dislocation coordinate in polar coordinate system
σ_{ij}	Components of stress
σ_0	Differential bulk tension
$\bar{\sigma}$	Stress induced by dislocations
$\tilde{\sigma}$	Stress in absence of crack
ϕ	unknown function
ω	prescribed fundamental function

1. Introduction

Fretting occurs when two bodies, pressed into contact, are subject to cyclic tangential loading, leading to local regions of cyclic slip even though the contact is notionally stuck. These cyclic slip displacements are typically caused by vibrations resulting in a large number of load cycles. We find the fretting regions to encourage fatigue crack nucleation, reducing

the fatigue life. The study of this phenomenon is referred to as fretting fatigue and is mainly concerned with the change of tractions and therefore the stress field in which cracks nucleate, caused by localised cyclic slip displacements. Additionally, fretting causes a modification of the surface geometry of the contacting bodies due to wear. Most studies of wear look at sliding contacts, where a relative rigid body motion between the two components is present and leads to much higher amplitudes of slip displacement compared to what we find for fretting contacts. Nevertheless, the localised region of cyclic displacements might lead to severe wear even for small amplitudes of slip, and we refer to this phenomenon as fretting wear. The process of wear in both scenarios, macroscopic sliding and localised cyclic slip, is similar in terms of surface particles being eroded from the contacting surfaces to produce wear debris. Although this is often done (Ding et al., 2004), it is *unrealistic* to tackle fretting wear problems employing traditional wear laws, for example, that proposed by Archard (1953), which are calibrated by experiments involving sliding contacts. The environment differs in the sense that for sliding contacts the contact region changes which might favour the escape of debris while the localised slip in a fretting contact leads to debris entrapment.

The surface modification and the corresponding change of contact tractions due to long-term wear have been considered for elastically similar bodies by Hills et al. (2009) for a Hertzian contact represented by half-planes and by Dini et al. (2008) for an axisymmetric Hertzian contact. Here, we intend to look at a semi-infinite representation of the contact edge of elastically similar bodies and find the modification of the contact tractions due to wear. In comparison to the earlier solutions for finite contacts the asymptotic form of the results in this study will allow us to incorporate the solution in a range of different incomplete contact geometries and hence add universality.

When looking at the near edge contact tractions of an incomplete contact we find the normal traction, $p(r)$, to be square root bounded with

$$L_I = \lim_{r \rightarrow 0} \frac{p(r)}{\sqrt{r}}, \quad (1)$$

being the asymptotic contact pressure multiplier and r is measured from the contact edge (Fig. 1(a)). Generally, L_I depends on the normal loading, P , as well as the geometry and example calibrations can be found from Dini and Hills (2004) and Dini et al. (2004) for a Hertzian and a flat and rounded contact, respectively.

Turning to the effect of tangential loading and assuming the contact to be fully stuck, as shown in Figure 1(a), for now, we expect a square root singular response in the shear traction, $q(r)$. This prompts us to define a shear traction stress intensity factor at the contact edge, K_{II}^e , with

$$K_{II}^e = \lim_{r \rightarrow 0} q(r) \sqrt{r}. \quad (2)$$

As K_{II}^e characterises the shear traction at the initial edge of the contact, we added the superscript ‘e’ to distinguish it from multipliers introduced at a later point and related to the state of stress at the wear boundary (Fig. 1(d)). The value of K_{II}^e depends on the tangential loading as well as the half-width of the finite contact, a , but is *independent* of

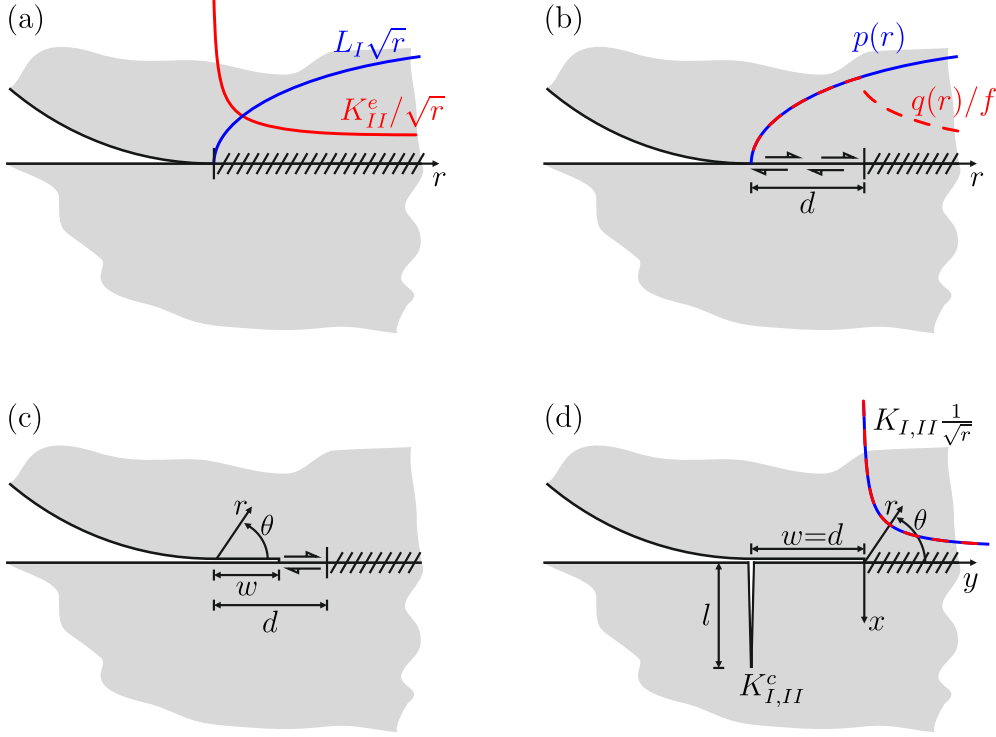


Figure 1: Incomplete contact a) in conditions of fully stuck, b) in partial slip c) with wear slit extending into the former slip zone and d) crack nucleating from the final wear zone.

the relative profile of the contacting bodies (Hills et al., 2016). We find

$$K_{II}^e = \frac{Q}{\pi\sqrt{2a}} + \frac{\sigma_0}{4}\sqrt{\frac{a}{2}}, \quad (3)$$

for the application of a shear force, Q , as well as a differential bulk tension, σ_0 .

Allowing for relative displacements between the contacting bodies, with a finite coefficient of friction, f , we find a slip zone close to the contact edge whose extent, d , is given by (Moore et al., 2018)

$$d = \frac{\Delta K_{II}^e}{fL_I}, \quad (4)$$

where ΔK_{II}^e is the range of shear loading under conditions of oscillatory shear force and bulk tension. Inside the slip zone, the shear traction will be bounded by $fp(r)$ whereas a corrective shear traction acts over the extent of the stick zone. The asymptotic contact tractions for an incomplete contact in partial slip, as shown in Figure 1(b), are then given by

$$p(r) = L_I\sqrt{r} \quad (5)$$

$$q(r) = fL_I \left(\sqrt{r} - \sqrt{r-d} \right) \quad (6)$$

where we adopted the usual convention of the normal traction being positive for compression and both the tractions have to be interpreted in terms of their real parts. Within the slip-region, $0 < r < d$, wear and the corresponding profile reduction will cause a reduction of the normal traction. Within the slip zone, a reduction of the normal traction will also change the shear traction which can be carried over the specific contact region. For an Archard type wear law, over time or a specific amount of load cycles, we expect wear to be proportional to the product of contact pressure and slip displacements, $p(r)h(r)$. It is not our intention, however, to describe wear as a time-dependent process, nor to recourse to any specific wear law. Instead, we intend to describe the long-term effect of wear as an asymptotic state. If wear proceeds long enough, eventually the profile reduction of the contacting bodies leads to a vanishingly small normal traction and a glancing contact establishes itself in the wear zone, i.e. all tractions vanish. The wear zone can be assumed to extend from the edge of the contact, where the initial slip displacements have their maximum, to a point, w , along the contact interface. The extent of the final wear zone, $0 \leq r \leq w$, is initially unknown, but it will be such that all slip has ceased and the remaining contact is fully stuck. Whenever the contact tractions outside the wear zone, $w < r$, give rise to partial slip (Fig. 1(c)), we expect the wear zone to continue to expand until just outside the wear zone the ratio of shear to normal traction is just less than the limiting condition, i.e.

$$\lim_{r \rightarrow w^+} \frac{q(r)}{p(r)} = f - \epsilon. \quad (7)$$

We find this to be the limiting condition as the wear zone cannot continue to grow if the contact is in a condition of stick just outside the wear zone (Fig. 1(d)). This asymptotic state of wear, and the corresponding modified state of stress around the contact edge, is of practical relevance if we look at conditions of severe wear in which the final state is reached after a small proportion of the components life. For such a case of severe wear, the propagation of fretting fatigue cracks can be assumed to mainly occur in a stress environment corresponding to the asymptotic state of wear.

2. Formulation

To account for the profile reduction caused by wear as well as the relative tangential displacement between the two bodies we introduce arrays of distributed dislocations along the wear zone, $0 \leq r \leq w$. The edge of the elastically similar contacting bodies, for an incomplete contact represented as half-planes, can be thought of as a semi-infinite crack. We find, first, the tractions caused by an array of distributed glide or climb edge dislocations of density $B_i(\rho)$ with $i = r, \theta$, respectively, positioned along a line drawn from the contact edge

$$\bar{\sigma}_{i\theta}(r) = \frac{2\mu}{\pi(\kappa + 1)} \int_0^w B_i(\rho) G_{i\theta}(r, \rho) d\rho, \quad (8)$$

where μ is the shear modulus of the contacting bodies and $\kappa = 3 - 4\nu$ is Kolosov's constant for plane strain with ν being Poisson's ratio. For an array of glide edge dislocations, $B_r(\rho)$,

the stress is found along the same line and $G_{rr\theta}(r, \rho)$ is given by Moore et al. (2018) as

$$G_{rr\theta}(r, \rho) = \sqrt{\frac{\rho}{r}} \frac{1}{r - \rho}. \quad (9)$$

The normal stress, $\bar{\sigma}_{\theta\theta}(r)$, caused by a corresponding array of climb edge dislocations, $B_\theta(\rho)$, is described by a similar Kernel function, i.e. $G_{\theta\theta\theta}(r, \rho) = G_{rr\theta}(r, \rho)$, and the problem is uncoupled in the sense that $G_{r\theta\theta}(r, \rho) = G_{\theta r\theta}(r, \rho) = 0$.

The normal and shear traction, $N(r)$ and $S(r)$, respectively, are given by two uncoupled algebraic equations

$$N(r) = L_I \sqrt{r} + \frac{2\mu}{\pi(\kappa + 1)} \frac{1}{\sqrt{r}} \int_0^w \frac{\sqrt{\rho} B_\theta(\rho)}{r - \rho} d\rho, \quad (10)$$

$$S(r) = f L_I \left(\sqrt{r} - \sqrt{r - d} \right) + \frac{2\mu}{\pi(\kappa + 1)} \frac{1}{\sqrt{r}} \int_0^w \frac{\sqrt{\rho} B_r(\rho)}{r - \rho} d\rho, \quad (11)$$

as a superposition of the bilateral tractions, $\tilde{\sigma}_{\theta\theta} = p(r)$ and $\tilde{\sigma}_{r\theta} = q(r)$, in the absence of the wear-slit, and the stress caused by the dislocations, $\bar{\sigma}_{\theta\theta}(r)$ and $\bar{\sigma}_{r\theta}(r)$, representing the wear-slit. We identify the unknown dislocation densities, $B_i(\rho)$, by the requirement that the worn contact faces are traction free, i.e. $N(r) = S(r) = 0$ for $0 \leq r \leq w$. This leads to

$$L_I \sqrt{r} = \frac{2\mu}{\pi(\kappa + 1)} \frac{1}{\sqrt{r}} \int_0^w \frac{\sqrt{\rho} B_\theta(\rho)}{\rho - r} d\rho \quad \text{for } 0 \leq r \leq w, \quad (12)$$

$$f L_I \left(\sqrt{r} - \sqrt{r - d} \right) = \frac{2\mu}{\pi(\kappa + 1)} \frac{1}{\sqrt{r}} \int_0^w \frac{\sqrt{\rho} B_r(\rho)}{\rho - r} d\rho \quad \text{for } 0 \leq r \leq w. \quad (13)$$

The equations differ only by a factor f on the left-hand side when $w \leq d$. With

$$s = 2 \frac{\rho}{w} - 1 \quad \text{and} \quad (14)$$

$$t = 2 \frac{r}{w} - 1, \quad (15)$$

we normalise the integral range in equations (12) and (13) to the interval $[-1 \quad 1]$, to derive

$$\int_{-1}^1 \sqrt{\frac{s+1}{t+1}} \frac{\hat{B}_\theta(s)}{s-t} ds = \sqrt{\frac{t+1}{2}}, \quad (16)$$

$$\int_{-1}^1 \sqrt{\frac{s+1}{t+1}} \frac{\hat{B}_r(s)}{s-t} ds = \begin{cases} \sqrt{\frac{t+1}{2}} & w \leq d \\ \sqrt{\frac{t+1}{2}} - \sqrt{\frac{t+1}{2} - \frac{d}{w}} & w > d \end{cases}, \quad (17)$$

for values of t such that $-1 \leq t \leq 1$, and where

$$\hat{B}_\theta(s) = \frac{2\mu}{\pi(\kappa + 1)} \frac{B_\theta(s)}{L_I \sqrt{w}}, \quad (18)$$

$$\hat{B}_r(s) = \frac{2\mu}{\pi(\kappa + 1)} \frac{B_r(s)}{f L_I \sqrt{w}}. \quad (19)$$

The different cases in equation (17) simply consider the real values of the left-hand side of equation (13), here separated for clarity. It is now easy to see, that for the case of a wear zone, $w \leq d$, the two equations (16) and (17) will have the same solution $\hat{B}_\theta(s) = \hat{B}_r(s)$, and consequently $B_r = fB_\theta$. Using this result in equations (10) and (11) leads

$$N(r) = L_I \sqrt{r} + \frac{2\mu}{\pi(\kappa + 1)} \frac{1}{\sqrt{r}} \int_0^w \frac{\sqrt{\rho} B_\theta(\rho)}{r - \rho} d\rho, \quad (20)$$

$$S(r) = fL_I \left(\sqrt{r} - \sqrt{r - d} \right) + \frac{2\mu}{\pi(\kappa + 1)} \frac{1}{\sqrt{r}} \int_0^w \frac{\sqrt{\rho} f B_\theta(\rho)}{r - \rho} d\rho, \quad (21)$$

for the normal and shear traction along the contact interface. We may use equation (8) to simplify equations (20) and (21) to

$$N(r) = L_I \sqrt{r} + \bar{\sigma}_{\theta\theta}(r), \quad (22)$$

$$S(r) = fL_I \left(\sqrt{r} - \sqrt{r - d} \right) + f\bar{\sigma}_{\theta\theta}(r), \quad (23)$$

and it is clear, that the stress caused by a profile reduction within the initial slip zone, will not change the fact that the shear traction will be a scaled version of the normal traction up to exactly the extent of the initial slip zone, d , after which the shear traction is such that the contact will be stuck in the region it was stuck before. Hence, a profile reduction due to wear does not affect the location of the stick-slip boundary. We have shown this for the assumption that the wear zone extends from the edge of the contact to a point, w , within the slip zone, and that within the wear zone all tractions have vanished. Following the same line of reasoning, it is however possible, to show that any reduction of the normal traction caused by wear and a corresponding profile reduction within the initial slip zone, will not affect the position of the initial stick-slip boundary. This is independent of the amount by which the normal traction is reduced (tensile normal tractions still excluded) as well as the exact position within the slip zone and is shown in more detail in Appendix A. As wear will start in the initial slip zone and continue until all tractions within the wear zone have vanished, but wear will never affect the position of the stick-slip boundary, it is clear that the initial size of the slip zone, d , will be the final extent of the wear zone, $w = d$. This corresponds to the results found by Hills et al. (2009) and Dini et al. (2008) for a finite contact description.

To find the tractions present for the worn configuration the two uncoupled singular integral equations of the first kind may be treated in the usual way using the method developed by Erdogan et al. (1973). We expect the solution to be bounded-singular and let

$$B_i(s) = \phi(s)\omega(s), \quad (24)$$

with

$$\omega(s) = \sqrt{\frac{1+s}{1-s}}. \quad (25)$$

Following the quadrature in Erdogan et al. (1973), the integral will be calculated in a numerical sense where the N integration and collocation points, s_i and t_k respectively, are

given by

$$s_i = \cos \left(\pi \frac{2i-1}{2N+1} \right) \quad i = 1, \dots, N \quad \text{and} \quad (26)$$

$$t_k = \cos \left(\pi \frac{2k}{2N+1} \right) \quad k = 1, \dots, N. \quad (27)$$

The following system of equations can be inverted to give the solutions $\phi(s)$ at the N integration points s_i (Hills et al., 2013). For example the calculation of the climb edge dislocation density reads

$$\pi \sum_{i=1}^N W_i \frac{\sqrt{s_i+1}}{s_i - t_k} \hat{\phi}_\theta(s_i) = \frac{1}{\sqrt{2}} (t_k + 1), \quad (28)$$

giving N equations with $k = 1, \dots, N$ for the N unknowns $\hat{\phi}_\theta(s_i)$. $\hat{\phi}_\theta(s)$, here, is defined as

$$\hat{\phi}_\theta(s) = \frac{2\mu}{\pi(\kappa+1)} \frac{\phi_\theta(s)}{L_I \sqrt{w}}, \quad (29)$$

and following equation (28) it is independent of the size of the wear zone, w . The weights W_i are given by

$$W_i = 2 \frac{1+s_i}{2N+1}. \quad (30)$$

The arranged climb edge dislocations will cause a singular normal traction outside the wear zone, $r > w$, which is characterised by the contact multiplier K_I , as shown in Figure 1(d). From Hills et al. (2013) we find¹

$$\begin{aligned} K_I &= \sqrt{w} \frac{2\mu}{(\kappa+1)} \phi_\theta(1) \\ \Leftrightarrow \frac{K_I}{L_I w} &= \pi \hat{\phi}_\theta(1), \end{aligned} \quad (31)$$

with $\hat{\phi}_\theta(1)$ calculated from $\hat{\phi}_\theta(s)$ by Krenk's interpolation (Krenk, 1975). As $\hat{\phi}_\theta(1)$ is independent of the extent of the wear zone, equation (31) represents a universal calibration between the initial normal contact multiplier, L_I , the length of the wear zone, w , and the resulting multiplier K_I , characterising the singularity at the tip of the wear zone. We find

$$\frac{K_I}{L_I} = \frac{w}{2}, \quad (32)$$

and note that K_I varies with the size of the wear zone, w , but not with the oscillating shear force. Correspondingly, the arranged glide edge dislocations will cause a singular

¹Note, that in difference to a classical crack tip stress intensity factor, for the contact multiplier we do not connect the tractions and the multiplier by a factor of $1/\sqrt{2\pi}$. Consequently, equation (31) is missing a factor of $\sqrt{2\pi}$ compared to what we find in Hills et al. (2013).

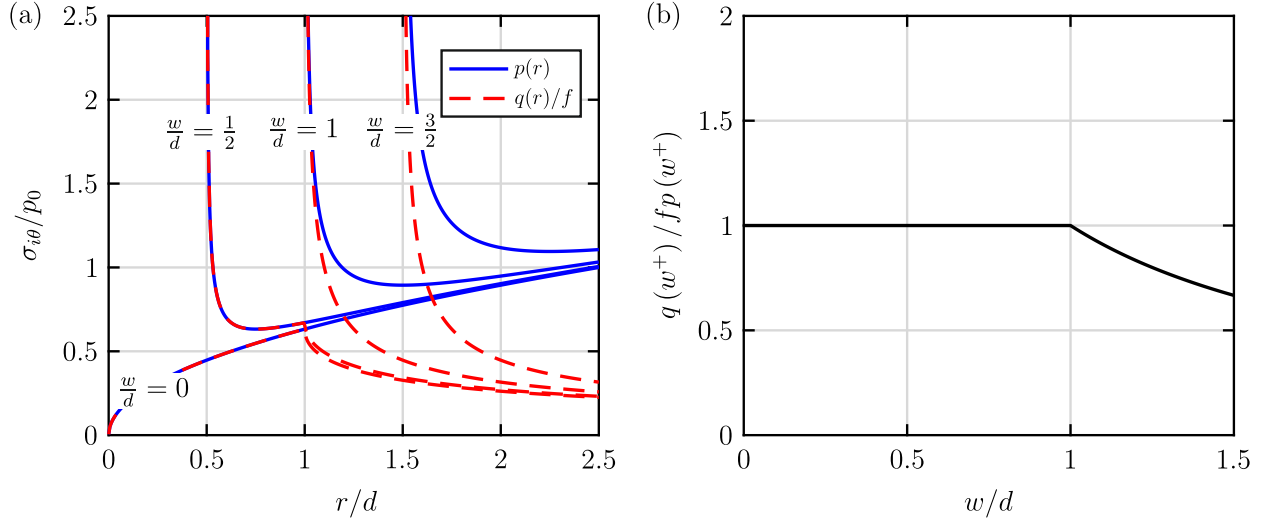


Figure 2: (a) Contact tractions for different extents of the wear zone w/d and (b) the ratio of tractions just outside the wear zone for a continuous variation of w/d .

shear traction outside the wear zone, $r > w$, which in turn is characterised by the contact multiplier K_{II} (Fig. 1(d)). Following similar steps to what we have done for the derivation of K_I in equations (29) to (32), we find relationship (32), with the left-hand side multiplied by $1/f$, to hold for the multiplier, K_{II} , for a specific extent of the wear zone $w \leq d$. K_{II} , however, does vary with the oscillating shear load. Using equation (4) we find it to be fully reversing with its amplitude being

$$\frac{K_{II}}{\Delta K_{II}^e} = \frac{1}{2} \frac{w}{d}, \quad (33)$$

such that the range of the multiplier characterising the stress at the wear-boundary is equal to the range of the multiplier defined at the initial contact, i.e. $\Delta K_{II} = \Delta K_{II}^e$, for $w = d$. For fully reversing tangential loads this also leads the same amplitude of the multipliers $K_{II} = K_{II}^e$, which with the asymptotic assumption $d \ll a$, corresponds to the results found by Hills et al. (2009) for the finite Hertzian contact.

3. Results

Although we identified the final size of the wear zone in the previous paragraph, our formulation in terms of distributed dislocations allows us to choose the extent, w , and we want to use this to visualise what we have shown mathematically before. Figure 2(a) shows the contact tractions, $p(r)$ and $q(r)$, for different ratios of the wear-boundary and the initial slip zone length, w/d . We find the initial tractions of the unworn contact for $w/d = 0$. For $w/d = 0.5$ we see that slip continues outside the wear zone with $q(r) = fp(r)$ for $w < r \leq d$, i.e. until the end of the initial slip zone. This is such that all points in the unworn contact region which were initially slipping are still in a state of partial slip, while all the points

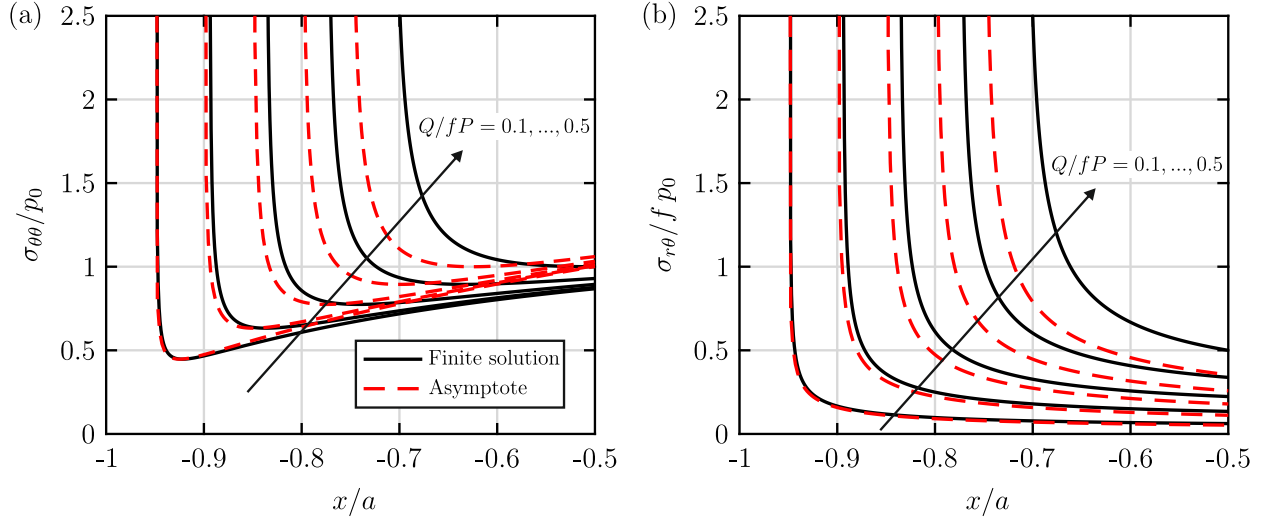


Figure 3: Comparison of asymptotic contact (a) normal and (b) shear traction with results for the finite description by Hills et al. (2009) for different ratios of tangential to normal loading $Q/fP = 0.1, \dots, 0.5$ (Legend in (a) applies to both subfigures).

in the initial stick-region are still stuck. We can immediately see that these states will not represent the final state of the wear-contact as wear will continue until all slip has ceased.

For the following two ratios of $w/d = 1, 1.5$ we cannot immediately see the ratio of tractions, $q(r)/fp(r)$ just outside the wear zone, $r \rightarrow w^+$, but plotting the traction ratio for a continuous variation of w/d visually confirms the result found in the last paragraph. If we choose $w < d$ the point just outside the wear zone will be in a state of slip, i.e. $q(r) = fp(r)$ for $r \rightarrow w^+$, and certainly wear will continue. If we increase the extent of the wear zone to $w > d$ we find the point outside the wear region to be in a condition of stuck, i.e. $q(r) < fp(r)$ for $r \rightarrow w^+$ (Fig. 2(b)).

We want to compare the results obtained here, found within an asymptotic formulation, to results for a finite description of the contact. Hills et al. (2009) found the finite solution for a Hertzian contact with a cylinder of radius R pressed into a half-space by a normal load, P , giving rise to a contact half-length, a . Subsequently, a fully reversing tangential load, of amplitude Q , is applied. The contact multiplier, L_I , for the specific contact geometry is given to (Dini and Hills, 2004)

$$L_I = \frac{2P}{\pi a} \sqrt{\frac{2}{a}}. \quad (34)$$

Figure 3 shows a comparison of the resulting wear tractions for the final state of wear, $w = d$, between the asymptotic results and the results found by Hills et al. (2009). For the comparison, x is measured from the centre of the finite contact, and, consequently, $x/a = -1$ denotes the edge of the initial contact. For different tangential loadings, $Q/fP = 0.1, \dots, 0.5$, Figure 3(a) shows the final normal tractions for the worn contact, where the finite results are shown as solid lines and the results obtained from the asymptotic description are represented by dashed lines. The corresponding results for the shear traction, at the point of maximum

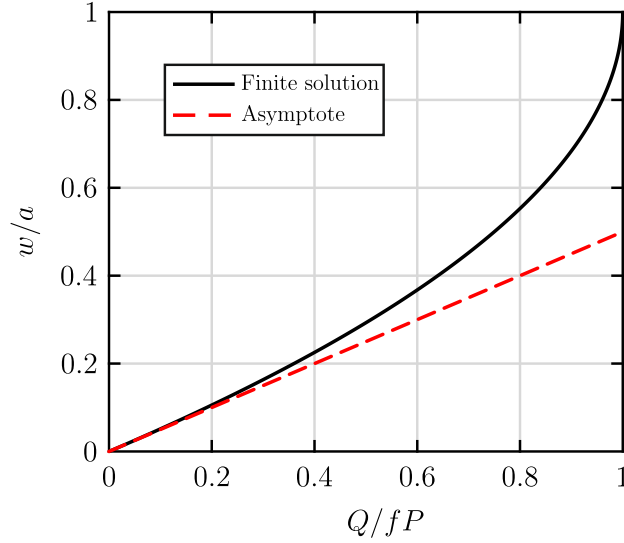


Figure 4: Extent of final wear zone for a Hertzian contact loaded by a tangential load Q/fP , calculated for the finite (solid) and the semi-infinite (dashed) consideration of the contact.

shear load, Q , are displayed in Figure 3(b) for the trailing edge.

We see that the quality of the asymptotic solution strongly depends on the ratio of tangential and normal loading, Q/fP . This follows the asymptotic description of a partial slip contact, which served as a starting point (c.f. equation (6)), and requires the slip zone to be small compared to the contact half-width, i.e. $d \ll a$ (Dini and Hills, 2004). The final size of the wear zone is plotted in Figure 4. We compare the extent of the wear zone, derived for the finite contact in Hills et al. (2009), plotted as solid lines, to the results from the semi-infinite (asymptotic) model of the contact edge (dashed). As for the contact tractions shown in Figure 3 we find very good agreement between the asymptote and the finite solution, for small values of tangential loading up to $Q/fP = 0.2$.

Although this comparison shows results for a Hertzian contact only, our asymptotic formulation allows us to incorporate the results in various incomplete contact settings as long as we know the asymptotic multiplier, L_I .

4. Fatigue cracks nucleating in the wear zone

The question arises, how wear, and the resulting tractions, affect the nucleation and propagation of cracks as shown in Figure 1(d). We will restrict ourselves to cracks that are short compared to any length characterising the finite contact so that they only see the asymptotic stress field. For convenience, we consider the point in the load cycle of maximum shear load, with multiplier K_{II} and we want to find the corresponding crack tip stress intensity factors. We can use the same procedure to find the range experienced by the crack tip stress intensity factors, for a range of ΔK_{II} .

We start with finding the stress along the potential crack line, resulting from the final contact tractions. We know that, close to the edge of the wear zone, both the tractions can

be described by the dominating square root singular term. For the final state of wear we find $K_I = fK_{II}$ and $K_{II} = \Delta K_{II}^e/2$ for the normal and shear traction multiplier, respectively. We assume the contact with all its tractions as well as the extent of the wear zone to be frozen and we can think of the wear-slit as a continuation of the semi-infinite crack in an infinite plane, as the two bodies are stuck together outside the wear zone, $r > w$. This enables us to use the Williams solution (Williams, 1952) to find the stress field in the (uncracked) lower body, which will now be described with the polar coordinate system having its origin at the wear-stick boundary and not at the initial edge of the contact as before (Fig. 1(d)).

We assume cracks to nucleate perpendicular to the surface and together with the crack we introduce a Cartesian coordinate system, whose origin also is at the wear-stick boundary. The x -axis is parallel to the crack and the y -axis aligned with the contact interface, as shown in Figure 1(d). For simplicity, we start looking at cracks nucleating from the edge of the final contact ($y = 0$ but not the location of the crack shown in Figure 1(d)). For a square root singular normal traction the complete bilateral stress field (in the absence of the crack) in polar coordinates as well as the stress along $y = 0$, are obtained by finding the eigenvector corresponding to the eigenvalue $\lambda = 1/2$ from the symmetric part of the Williams solution as

$$\begin{bmatrix} \tilde{\sigma}_{rr}(r, \theta) \\ \tilde{\sigma}_{\theta\theta}(r, \theta) \\ \tilde{\sigma}_{r\theta}(r, \theta) \end{bmatrix} = -\frac{1}{4}K_I \frac{1}{\sqrt{r}} \begin{bmatrix} 5 \cos\left(\frac{\theta}{2}\right) - \cos\left(\frac{3\theta}{2}\right) \\ 3 \cos\left(\frac{\theta}{2}\right) + \cos\left(\frac{3\theta}{2}\right) \\ \sin\left(\frac{\theta}{2}\right) + \sin\left(\frac{3\theta}{2}\right) \end{bmatrix} = \frac{1}{2\sqrt{2}}K_I \frac{1}{\sqrt{r}} \begin{bmatrix} -3 \\ -1 \\ 1 \end{bmatrix}_{\theta=-\frac{\pi}{2}}. \quad (35)$$

Analogously we find the stress corresponding to the square-root singular shear traction from the anti-symmetric part of the Williams solution (for the same eigenvalue $\lambda = 1/2$) to

$$\begin{bmatrix} \tilde{\sigma}_{rr}(r, \theta) \\ \tilde{\sigma}_{\theta\theta}(r, \theta) \\ \tilde{\sigma}_{r\theta}(r, \theta) \end{bmatrix} = \frac{1}{4}K_{II} \frac{1}{\sqrt{r}} \begin{bmatrix} -5 \sin\left(\frac{\theta}{2}\right) + 3 \sin\left(\frac{3\theta}{2}\right) \\ -3 \sin\left(\frac{\theta}{2}\right) - 3 \sin\left(\frac{3\theta}{2}\right) \\ \cos\left(\frac{\theta}{2}\right) + 3 \cos\left(\frac{3\theta}{2}\right) \end{bmatrix} = \frac{1}{2\sqrt{2}}K_{II} \frac{1}{\sqrt{r}} \begin{bmatrix} 1 \\ 3 \\ -1 \end{bmatrix}_{\theta=-\frac{\pi}{2}}. \quad (36)$$

The idea is, now, to find a calibration between the crack tip stress intensity factors K_I^c and K_{II}^c and the contact multipliers K_I and K_{II} , characterising the stress field around the edge of the final contact. We follow a similar approach to that used for the calibration between L_I and K_I in §2, only this time we introduce glide and climb edge dislocations along the crack line to ensure the crack faces being traction free with $N(x) = S(x) = 0$ for $0 \leq x \leq l$, where l is the crack length. Corresponding to equations (10) and (11), the normal and shear traction along the crack line are now given by

$$N(x) = \tilde{\sigma}_{yy}(x, 0) + \frac{2\mu}{\pi(\kappa + 1)} \int_0^l B_y(\xi) G_{yyy}(x, \xi) d\xi, \quad (37)$$

and

$$S(x) = \tilde{\sigma}_{xy}(x, 0) + \frac{2\mu}{\pi(\kappa + 1)} \int_0^l B_x(\xi) G_{xyy}(x, \xi) d\xi. \quad (38)$$

For the coordinate systems defined as in Figure 1(d), we find $\tilde{\sigma}_{yy}(x, 0) = \tilde{\sigma}_{\theta\theta}(r, -\pi/2)$ and $\tilde{\sigma}_{xy}(x, 0) = \tilde{\sigma}_{r\theta}(r, -\pi/2)$. This allows us to use either equation (35) or (36) for the bilateral

stresses, depending on if we want to find the calibration for K_I or K_{II} , respectively. For notational convenience we will describe the following steps for the calibration between K_I and the crack tip stress intensity factors only, but they will be essentially similar for the calibration of K_{II} .

The crack, and therefore the dislocations will be introduced in the lower body, which itself is represented by a half-plane. The corresponding kernel functions are (Hills et al., 2013)

$$G_{yyy} = G_{xxy} = \frac{1}{x - \xi} - \frac{1}{x + \xi} - \frac{2\xi}{(x + \xi)^2} + \frac{4\xi^2}{(x + \xi)^3}. \quad (39)$$

Using kernel functions for dislocations in a half-plane is an approximation in the sense that the stress caused by the arranged dislocations, and therefore the change of the stress field due to the presence of the crack will not affect the contact traction. While Munisamy et al. (1995) have shown this effect to be small, it provides us with a closed form of the kernel function, as specified in equation (39), and we follow the procedure introduced by Araújo and Nowell (1999).

We normalise the integral range, similar to equations (14) and (15), only, this time using the crack length, l , instead of w . Following the same numerical approach we used in §2, and after dividing equations (37) and (38) by K_I/\sqrt{l} , we are able to find a general solution for the unknowns

$$\hat{\phi}_j(s) = \frac{2\mu}{\pi(\kappa + 1)} \frac{\sqrt{l}\phi_j(s)}{K_I}, \quad (40)$$

with $j = x, y$ (compare to equation (27)). Again, we find the dislocation density at the crack tip by Krenk's interpolation (Krenk, 1975), and the crack tip stress intensity factors to (Hills et al., 2013)

$$\begin{aligned} K_{I,II}^c &= \sqrt{2\pi}\sqrt{l} \frac{2\mu}{(\kappa + 1)} \phi_j(1) \\ \Leftrightarrow \frac{K_{I,II}^c}{K_I} &= \pi\sqrt{2\pi}\hat{\phi}_j(1), \end{aligned} \quad (41)$$

where we find K_I^c from ϕ_x and K_{II}^c from ϕ_y . The corresponding calibrations for K_{II} , are then found by choosing equation (36) for the bilateral tractions $\tilde{\sigma}_{iy}$ in equations (37) and (38). The corresponding calibration matrix is identified to

$$\begin{Bmatrix} K_I^c \\ K_{II}^c \end{Bmatrix} = \begin{bmatrix} -1.209 & 3.628 \\ 1.209 & -1.209 \end{bmatrix} \begin{Bmatrix} K_I \\ K_{II} \end{Bmatrix}, \quad (42)$$

and we point out, again, that this is the result for the crack nucleating from the boundary of the wear zone.

For the crack nucleating from the edge of the initial contact, as shown in Figure 1(d) (or any point within the wear zone), we need to find the stress along a remote line with a distance d . The substitutions $r = \sqrt{x^2 + d^2}$ and $\theta = \arctan(x/d) - \pi$, in equation (35), together with a rotation of the state of stress by an angle $\varphi = -(\pi/2 + \theta)$, to align with

the x - y -system, yield expressions for the tractions along the potential crack line caused by a square root singular normal traction, to

$$\tilde{\sigma}_{yy}(x, -d) = \frac{1}{2\sqrt{2}} K_I \sqrt{\frac{\sqrt{x^2 + d^2} - d}{x^2 + d^2}} \left(1 + \frac{d}{\sqrt{x^2 + d^2}} + \frac{2d^2}{x^2 + d^2} \right), \quad (43)$$

and

$$\tilde{\sigma}_{xy}(x, -d) = \frac{1}{2\sqrt{2}} K_I \sqrt{\frac{\sqrt{x^2 + d^2} + d}{x^2 + d^2}} \left(1 + \frac{d}{\sqrt{x^2 + d^2}} - \frac{2d^2}{x^2 + d^2} \right). \quad (44)$$

Analogously, we find the tractions along the potential crack line caused by a square root singular shear traction to

$$\tilde{\sigma}_{yy}(x, -d) = \frac{1}{2\sqrt{2}} K_{II} \sqrt{\frac{\sqrt{x^2 + d^2} + d}{x^2 + d^2}} \left(3 - \frac{d}{\sqrt{x^2 + d^2}} + \frac{2d^2}{x^2 + d^2} \right), \quad (45)$$

and

$$\tilde{\sigma}_{xy}(x, -d) = \frac{1}{2\sqrt{2}} K_{II} \sqrt{\frac{\sqrt{x^2 + d^2} - d}{x^2 + d^2}} \left(1 + \frac{d}{\sqrt{x^2 + d^2}} + \frac{2d^2}{x^2 + d^2} \right). \quad (46)$$

As the bilateral tractions, (43) to (46), the calibration will now depend on the ratio of crack length and remote distance, d/l , i.e.

$$\begin{Bmatrix} K_I^c \\ K_{II}^c \end{Bmatrix} = \begin{bmatrix} -1.209 g_I^1(d/l) & 3.628 g_{II}^1(d/l) \\ 1.209 g_I^2(d/l) & -1.209 g_{II}^2(d/l) \end{bmatrix} \begin{Bmatrix} K_I \\ K_{II} \end{Bmatrix}, \quad (47)$$

where $g_{I,II}^{1,2} = 1$ for $d/l = 0$ (c.f. equation (42)). For a varying ratio $0 \leq d/l \leq 100$ the evaluated functions $g_{I,II}^{1,2}$, representing the calibration between crack tip stress intensity factors K_I^c and K_{II}^c and contact multipliers K_I and K_{II} , are shown in Figure 5. We find the biggest influence of the contact tractions on the crack tip stress intensity factors, close to the singularity at the edge of the final contact. If the crack length, l , is short compared to the remote distance, d , we find the influence of the contact shear traction on the mode I crack tip stress intensity factor, to dominate. Each point in Figure 5, represents the evaluation of the singular integral equations (37) and (38), where we chose a specific ratio, d/l . Even though we are not able to find closed-form expressions for $g_{I,II}^{1,2}$, here, we want to fit rational functions to the results obtained for discrete values of d/l . These rational functions consist of polynomials over polynomials of the form

$$g_{I,II}^{1,2} \left(\frac{d}{l} \right) \approx \frac{\sum_{j=0}^5 p_j \left(\frac{d}{l} \right)^j}{\sum_{j=0}^5 q_j \left(\frac{d}{l} \right)^j} \quad (48)$$

We used the *Matlab* build in function `fit()` to identify the different coefficients. The highest coefficient, q_i , is generally chosen to 1, and a coefficient p_i or $q_i = 0$, represents the choice of a

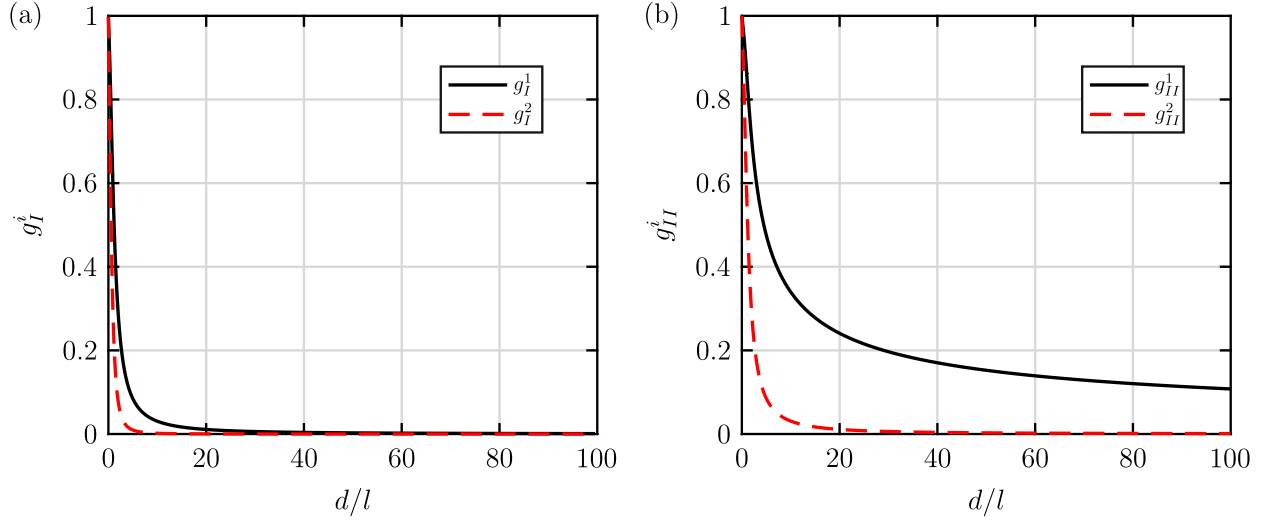


Figure 5: Remote calibration between crack tip stress intensity factors $K_{I,II}^c$ and (a) a singular normal traction K_I by means of $g_I^{1,2}$ and (b) a singular shear traction K_{II} by means of $g_{II}^{1,2}$.

Calibration	p_5	p_4	p_3	p_2	p_1	p_0
g_I^1	0	0.046	7.645	50.94	32.43	45.19
g_I^2	0	0	5.00e-4	-1.26e-3	4.457	19.32
g_{II}^1	6.83e-3	55.77	1.33e4	1.84e5	2.03e4	3.72e5
g_{II}^2	0	0.045	7.645	50.94	32.43	45.19
	q_5	q_4	q_3	q_2	q_1	q_0
g_I^1	1	28.26	48.85	69.06	47.24	45.17
g_I^2	0	1	23.85	21.1	23.49	19.31
g_{II}^1	1	1157	6.53e4	1.85e5	6.05e4	3.72e5
g_{II}^2	1	28.26	48.85	69.06	47.24	45.17

Table 1: Identified coefficients for the fit of rational functions to the results of the remote calibration.

lower order for the corresponding polynomial, rather than the result of the fit. Furthermore, the constraint $q_i \geq 0$ ensures the avoidance of singularities. The identified coefficients for the four functions $g_{I,II}^{1,2}$ are listed in table 1.

The above found calibrations enable us to find the crack tip stress intensity factor for a crack nucleating from the edge of the initial contact to

$$\frac{K_I^c}{\Delta K_{II}^e} = -\frac{1}{2} \left(1.209 f g_I^1 \left(\frac{d}{l} \right) - 3.628 g_{II}^1 \left(\frac{d}{l} \right) \right), \quad (49)$$

and

$$\frac{K_{II}^c}{\Delta K_{II}^e} = \frac{1}{2} \left(1.209 f g_I^2 \left(\frac{d}{l} \right) - 1.209 g_{II}^2 \left(\frac{d}{l} \right) \right), \quad (50)$$

where we used $K_I = f K_{II}$ and $K_{II} = \Delta K_{II}^e / 2$ together with equation (47) and normalised the resulting relations in terms of the range of the initial contact shear multiplier, ΔK_{II}^e ,

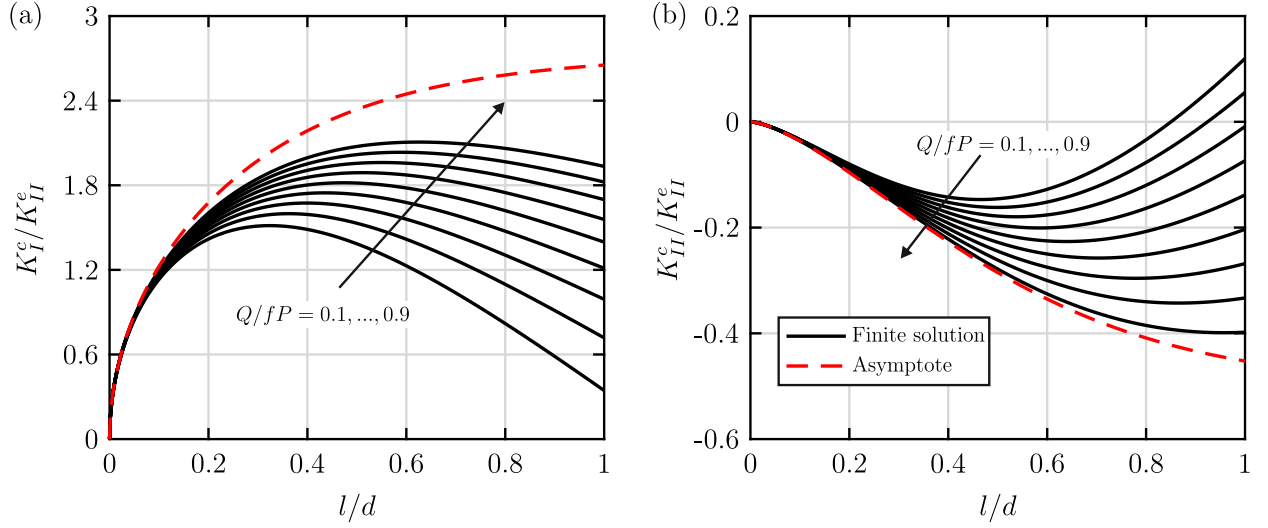


Figure 6: Comparison of asymptotic and finite results of crack tip stress intensity factors a) K_I^c and b) K_{II}^c for a crack nucleating from the initial edge of the contact. Different ratios of tangential loading, $Q/fP = 0.1, \dots, 0.9$, are considered ($f = 0.75$; Legend in (b) applies to both subfigures).

which is given by equation (3). d still denotes the initial slip zone length (4), for cracks nucleating from the edge of the initial contact but may be chosen freely to describe cracks nucleating from within the wear zone. We want to compare the results found from equations (49) and (50), for cracks nucleating in the asymptotic subsurface stress field, to results for cracks seeing the stress field corresponding to the finite representation of the contact. We find the finite tractions (as for the comparison in §3) from Hills et al. (2009). For brevity, we do not want to derive the subsurface stress field for the finite contact, here, but equations for obtaining it from the contact tractions can be found from Vázquez et al. (2012). The crack tip stress intensity factors for the finite solution is found by replacing the bilateral stress, $\tilde{\sigma}_{iy}$, in equations (37) and (38) by the stress found for the finite description of the subsurface stress field. Figure 6 shows, for different ratios of tangential loading, $Q/fP = 0.1, \dots, 0.9$, the crack tip stress intensity factor corresponding to the asymptotic considerations, introduced here, to the results we find for a finite description of the contact and the corresponding stress field.

We find good agreement as long as the crack length, l , is short compared to the remote distance, d , with $l < 0.15d$. For the crack growing from the contact interface, eventually reaching a region where the subsurface stress field is not sufficiently represented by the asymptotic solution, the crack tip stress intensity factor can not be found from the asymptotic considerations any longer. For the chosen normalisation, we find the results corresponding to the asymptotic description, to be independent of the ratio of normal and tangential loading, Q/fP . Furthermore, as for the asymptotic representation of the contact traction, the results shown in Figure 6 can be incorporated in any incomplete contact geometry as long as we know the geometry dependent normal multiplier L_I .

5. Conclusion

We have considered a general incomplete contact edge subject to oscillatory tangential loading originating from a shear load, Q , and a differential bulk tension, σ_0 . With a semi-infinite consideration of the contact edge, distributed dislocations have been used to account for the profile reduction due to wear. The results derived are not connected to a specific wear law and no attempt was made to describe the growth of the wear zone in terms of the number of experienced load cycles. The final relations allow us to characterise the singularities in normal and shear traction close to the boundary of the wear zone, in terms of a calibration between the corresponding contact multipliers, K_I and K_{II} , and those at the initial edge of the unworn contact, L_I and K_{II}^e . A comparison with a finite Hertzian contact shows good agreement as long as the extent of the wear zone is short compared to the contact half-width.

Based on the asymptotic form of the contact tractions, we found the subsurface stress field corresponding to the final state of the worn contact. Calibrations between crack tip stress intensity factors and the multipliers characterising the contact tractions are given for cracks nucleating from the initial contact interface. The crack might nucleate at the initial edge of the contact, or anywhere within the wear zone. The accuracy of the asymptotic crack tip stress intensity factor calibration depends on the crack length and the distance to the edge of the worn contact. Both the calibration for the worn contact tractions as well as for the crack tip stress intensity factors can be incorporated into different incomplete contact problems, as long as the geometry dependent asymptotic multiplier, L_I , is known.

Acknowledgements

N. Cwiekala and D. A. Hills thank Rolls-Royce plc and the EPSRC for the support under the Prosperity Partnership Grant ‘Cornerstone: Mechanical Engineering Science to Enable Aero Propulsion Futures’, Grant Ref: EP/R004951/1.

Appendix A. Location of stick-slip boundary for arbitrary amounts of wear

We start by looking at the asymptotic representation of a partial slip contact. The tractions present from the edge can be expressed as

$$\sigma_{\theta\theta}(r) = p(r), \tag{A.1}$$

$$\sigma_{r\theta}(r) = \begin{cases} fp(r) & 0 < r < d \\ fp(r) + q_c(r) & r > d \end{cases}, \tag{A.2}$$

where r is measured from the edge of the contact and we find $\sigma_{r\theta}(r) = f\sigma_{\theta\theta}(r)$ within the slip zone, $0 < r < d$, while a corrective shear traction, q_c ensures $\sigma_{r\theta}(r) < f\sigma_{\theta\theta}(r)$ within the stick zone, $r > d$.

We want to show that the position of the stick-slip boundary remains unchanged for arbitrary amounts of wear at any position within the initial slip zone. Let us suppose that within the slip zone our contact experiences wear over an arbitrary interval $[a \ b]$,

$0 \leq a, b \leq d$. The reduction of the normal traction, caused by a corresponding profile reduction, may be expressed as $p'(r)$ for $a \leq r \leq b$, where the condition $p(r) + p'(r) \geq 0$, expresses the fact, that we can never find a tension between the two bodies. We can find the dislocations representing the corresponding profile reduction from

$$p'(r) = \frac{2\mu}{\pi(\kappa + 1)} \int_a^b B_\theta(\rho) G_{\theta\theta\theta}(r, \rho) d\rho \quad \text{for } a \leq r \leq b. \quad (\text{A.3})$$

Within the slip zone, we generally find $\sigma_{r\theta}(r) = f\sigma_{\theta\theta}(r)$. It is clear then, that a reduction of the normal traction will cause a corresponding reduction in the shear traction with $q'(r) = fp'(r)$, and we may find the corresponding distribution of glide edge dislocations, representing the relative slip displacements by

$$fp'(r) = \frac{2\mu}{\pi(\kappa + 1)} \int_a^b B_r(\rho) G_{rr\theta}(r, \rho) d\rho \quad \text{for } a \leq r \leq b. \quad (\text{A.4})$$

For $G_{\theta\theta\theta}(r, \rho) = G_{rr\theta}(r, \rho)$, we find the solutions of equations (A.3) and (A.4), in terms of the dislocation densities, to be related via $B_r(\rho) = fB_\theta(\rho)$. The tractions, $\bar{\sigma}_{\theta\theta}(r)$ and $\bar{\sigma}_{r\theta}(r)$, caused by these dislocations, outside the interval $a \leq r \leq b$, are then given by equation (8) to

$$\bar{\sigma}_{\theta\theta}(r) = \frac{2\mu}{\pi(\kappa + 1)} \int_a^b B_\theta(\rho) G_{\theta\theta\theta}(r, \rho) d\rho \quad \text{and} \quad (\text{A.5})$$

$$\bar{\sigma}_{r\theta}(r) = \frac{2\mu}{\pi(\kappa + 1)} \int_a^b B_r(\rho) G_{rr\theta}(r, \rho) d\rho. \quad (\text{A.6})$$

Again, using $G_{\theta\theta\theta}(r, \rho) = G_{rr\theta}(r, \rho)$ as well as $B_r(\rho) = fB_\theta(\rho)$, we find $\bar{\sigma}_{r\theta}(r) = f\bar{\sigma}_{\theta\theta}(r)$. The total contact tractions are given by a superposition of the initial tractions (A.1) and (A.2), and those caused by the introduced distributions of dislocations

$$\sigma_{\theta\theta}(r) = p(r) + \bar{\sigma}_{\theta\theta}(r), \quad (\text{A.7})$$

$$\sigma_{r\theta}(r) = \begin{cases} fp(r) + f\bar{\sigma}_{\theta\theta}(r) & 0 < r < d \\ fp(r) + q_c(r) + f\bar{\sigma}_{\theta\theta}(r) & r > d \end{cases}. \quad (\text{A.8})$$

Consequently we find $\sigma_{r\theta}(r) = f\sigma_{\theta\theta}(r)$ within the initial slip zone, $0 < r < d$, while $\sigma_{r\theta}(r) < f\sigma_{\theta\theta}(r)$ within the initial stick zone, $r > d$, such that the position of the stick-slip boundary is not affected by wear.

References

- Araújo, J., Nowell, D., 1999. Analysis of pad size effects in fretting fatigue using short crack arrest methodologies. *International Journal of Fatigue* 21, 947–956.
- Archard, J., 1953. Contact and rubbing of flat surfaces. *Journal of applied physics* 24, 981–988.
- Ding, J., Leen, S., McColl, I., 2004. The effect of slip regime on fretting wear-induced stress evolution. *International Journal of Fatigue* 26, 521–531.

- Dini, D., Churchman, C., Rajasekaran, R., Hills, D., 2004. A correlation of the process zone properties in complete, incomplete and almost complete fretting contacts. *International journal of mechanical sciences* 46, 491–508.
- Dini, D., Hills, D.A., 2004. Bounded asymptotic solutions for incomplete contacts in partial slip. *International journal of solids and structures* 41, 7049–7062.
- Dini, D., Sackfield, A., Hills, D., 2008. An axi-symmetric hertzian contact subject to cyclic shear and severe wear. *Wear* 265, 1918–1922.
- Erdogan, F., Gupta, G.D., Cook, T., 1973. Numerical solution of singular integral equations, in: *Methods of analysis and solutions of crack problems*. Springer, pp. 368–425.
- Hills, D., Fleury, R., Dini, D., 2016. Partial slip incomplete contacts under constant normal load and subject to periodic loading. *International Journal of Mechanical Sciences* 108, 115–121.
- Hills, D., Sackfield, A., Paynter, R., 2009. Simulation of fretting wear in halfplane geometries: part 1—the solution for long term wear. *Journal of tribology* 131.
- Hills, D.A., Kelly, P., Dai, D., Korsunsky, A., 2013. *Solution of crack problems: the distributed dislocation technique*. volume 44. Springer Science & Business Media.
- Krenk, S., 1975. On the use of the interpolation polynomial for solutions of singular integral equations. *Quarterly of Applied Mathematics* 32, 479–484.
- Moore, M., Ramesh, R., Hills, D., Barber, J., 2018. Half-plane partial slip contact problems with a constant normal load subject to a shear force and differential bulk tension. *Journal of the Mechanics and Physics of Solids* 118, 245–253.
- Munisamy, R., Hills, D., Nowell, D., 1995. An analysis of coupling between plane cracks and contacts. *European journal of mechanics. A. Solids* 14, 55–71.
- Vázquez, J., Navarro, C., Domínguez, J., 2012. A new method for obtaining the stress field in plane contacts. *International Journal of Solids and Structures* 49, 3659–3665.
- Williams, M., 1952. Stress singularities resulting from various boundary conditions in angular corners of plates in extension. *Journal of applied mechanics* 19, 526–528.